APRIL 2011

SAN FRANCISCO ESTUARY & WATERSHED SCIENCE

Sponsored by the Delta Science Program and the UC Davis John Muir Institute of the Environment

A Tree-Ring Reconstruction of the Salinity Gradient in the Northern Estuary of San Francisco Bay

David W. Stahle[1*], R. Daniel Griffin[1,4], Malcolm K. Cleaveland[1], Jesse R. Edmondson[1], Falko K. Fye[1], Dorian J. Burnette[1], John T. Abatzoglou[2], Kelly T. Redmond[3], David M. Meko[4], Micheal D. Dettinger[5], Daniel R. Cayan[5], Matthew D. Therrell[6]

ABSTRACT

Blue oak tree-ring chronologies correlate highly with winter–spring precipitation totals over California, with Sacramento and San Joaquin river stream flow, and with seasonal variations in the salinity gradient in San Francisco Bay. The convergence of fresh and saline currents can influence turbidity, sediment accumulation, and biological productivity in the estuary. Three selected blue oak chronologies were used to develop a 625-year-long reconstruction of the seasonal salinity gradient, or low salinity zone (LSZ), which provides a unique perspective on the interannual-to-decadal variability of this important estuarine habitat indicator. The reconstruction was calibrated with instrumental LSZ data for the winter–spring season, and explains 73% of the variance in the February–June position of the LSZ from 1956 to 2003. Because this calibration period post-dates the sweeping changes that have occurred to land cover, channel morphology, and natural streamflow regimes in California, the reconstruction provides an idealized estimate for how the LSZ might have fluctuated under the seasonal precipitation variations of the past 625 years, given the modern geometry and bathymetry of the estuary and land cover across the drainage basin. The February–June season integrates precipitation and runoff variability during the cool season, and does not extend into the late-summer dry season when LSZ extremes can negatively affect Sacramento–San Joaquin Delta (Delta) agriculture and some aquatic organisms. However, there is such strong inter-seasonal persistence in the instrumental LSZ data that precipitation totals during the cool season can strongly pre-condition LSZ position in late summer. The 625-year-long reconstruction indicates strong interannual and decadal variability, the frequent recurrence of consecutive 2-year LSZ maxima and minima, large-scale ocean atmospheric forcing, and an interesting asymmetrical influence of warm El Niño–Southern Oscillation (ENSO) events.

* Corresponding author: *dstahle@uark.edu*
[1] Tree-Ring Laboratory, Department of Geosciences, Ozark Hall 113, University of Arkansas, Fayetteville, AR 72701
[2] Department of Geography, University of Idaho, Moscow, ID 83844-2130
[3] Western Regional Climate Center, Desert Research Institute, Reno, NV 89512-1095
[4] Laboratory of Tree-Ring Research, University of Arizona, Tucson, AZ 82721 (Current address for R. Daniel Griffin.)
[5] Scripps Institution of Oceanography, United States Geological Survey, University of California, San Diego, LaJolla, CA
[6] Geography and Environmental Resources, Southern Illinois University, Carbondale, IL 62901

KEY WORDS

blue oak, *Quercus douglasii*, tree rings, dendrochronology, low salinity zone, San Francisco Bay, estuarine habitat, paleoclimatology

INTRODUCTION

Natural and anthropogenic factors dictate modern water-quality conditions in the San Francisco Bay–Delta ecosystem (Peterson and others 1995; Knowles 2002; Kimmerer 2004). Precipitation over San Francisco Bay's drainage basin and subsequent freshwater outflow from the Sacramento–San Joaquin Delta (Delta) governs much of the seasonal-to-interannual variability in the position of the longitudinal salinity gradient in the northern estuary (Conomos 1979). The estuarine salinity gradient is usually steepest in Suisun Bay, where Delta outflow and the location of the salt field correlate with many biological variables (Jassby and others 1995; Kimmerer 2004; Enright and Culberson 2009). During wet winters with high runoff Suisun Bay is freshened and the gradient between fresh and saline water masses is forced seaward. During drought years with low streamflow, saline conditions intrude landward into the upper estuary. Reservoir storage and the export of freshwater from the Sacramento–San Joaquin system for agricultural, industrial, and municipal supplies have altered the natural runoff regime into the estuary (Nichols and others 1986), and freshwater transfer through the Delta has changed seasonal water clarity (Nobriga and others 2008). Many native and introduced organisms are sensitive to the aquatic habitat changes that result from net freshwater inflow to the estuary, and some organisms are in decline due to water-quality changes associated with drought and freshwater export (Jassby and others 1995).

An index of the longitudinal salinity gradient has been developed to measure changes in estuarine habitat conditions associated with variations in freshwater inflow from the Sacramento and San Joaquin rivers (Jassby and others 1995). The position of the salinity gradient is measured as the distance from the Golden Gate, up the axis of the estuary, to the point where the near-bottom water salinity concentration is 2 psu (practical salinity units, or 2‰, Jassby and others 1995; Monismith and others 2002). The position of this near-bottom isohaline, or low salinity zone (LSZ), correlates with several of the physical, chemical, and biological properties of the estuary, and can be managed, in part, by controlling freshwater export from the Sacramento–San Joaquin River system, especially during the dry, low-flow summer season.

Figure 1 This map of San Francisco Bay illustrates the mean position of the LSZ during the instrumental period from 1956–2003 in km, which was 67.3 km from the Golden Gate up the northern arm of the estuary. The February–June LSZ maxima and minima during the instrumental era were 92.2 and 49.2 km (1977 and 1983, respectively), and 90.0 and 37.7 km in the 625-year reconstruction (1976 and 1983, respectively).

The influence of precipitation over river discharge, Delta outflow, and the longitudinal salinity gradient also controls the growth of climate-sensitive blue oak trees (*Quercus douglasii*), which are widely distributed across San Francisco Bay's drainage basin. Because of this joint response to seasonal precipitation totals, past precipitation amounts, river discharge, and the resulting estuarine salinity gradient can be reconstructed. In this paper, we use three selected blue oak chronologies to reconstruct the seasonal position of the LSZ in the northern reach of San Francisco Bay for the past 625 years.

The LSZ can equate with the geographical location of the null point or null zone in some estuaries, where river-driven freshwater flow and tidally dispersed salinity motions balance and are associated with high turbidity, sediment accumulation, and biological productivity—marking a sharp transition between aquatic species composition of upper and lower estuaries (Miller 1983; Schemel and others 1984). However, the null zone in the northern estuary of San Francisco Bay (Suisun Bay) is less tightly related to freshwater flow rate, especially high flows, because the water column can become stratified in response to spatial changes in water depth and strong tidal motions (Monismith and others 2002). Nevertheless, freshwater inflow is important to biological productivity in the northern estuary and can mediate algal, planktonic, and fisheries production (Schemel and others 1984; Jassby and others 1995).

The influence of precipitation over California on freshwater inflow and estuarine salinity in San Francisco Bay has been described by Dettinger and Cayan (2003) and Enright and Culberson (2009). Enright and Culberson (2009) used an average of 13 precipitation-recording stations to compile an index of how precipitation has forced estuarine processes monthly and by water year. Their regional index averages climate variability across the sub-basins of the drainage network (e.g., Dettinger and others 1998), and emphasizes the combined effect of basin-wide precipitation on Delta outflow during the nearly 100 years of instrumental observations. In a similar manner, long precipitation-sensitive proxies can provide insight into the natural climate-driven variability of inflow, and the position of the salinity gradient during the late Holocene, apart from the artificial regulation of the Sacramento–San Joaquin hydraulic system (e.g., Malamud–Roam and others 2007).

Blue oak is an endemic California hardwood widely distributed across San Francisco Bay's drainage basin (Figures 2 and 3). It forms the lower forest border, and in moisture-limited sites is one of the most precipitation-sensitive tree species yet discovered (Meko and others 2001; Stahle and others 2001). Long tree-ring chronologies derived from these ancient blue oak can provide an intricate record of hydroclimatic

Figure 2 This 300-year-old blue oak tree at Rock Springs Mountain is typical of the ancient climate-sensitive blue oak found widely across the foothills of the Coast Ranges, Cascades, and Sierra Nevada.

variability over the drainage basin of San Francisco Bay for the past several centuries.

Freshwater flow into the Bay–Delta ecosystem and the index of the LSZ (referred to as X_2 by Jassby and others 1995), are regulated through the State Water Resources Control Board Decision 1641 (SWRCB 1995), with research input from the California Bay–Delta Authority (CBDA). Regulation of the system is challenged by competing interests, including water export for agricultural and municipal supplies in southern California, the maintenance of minimum flows in the Delta to supply irrigation

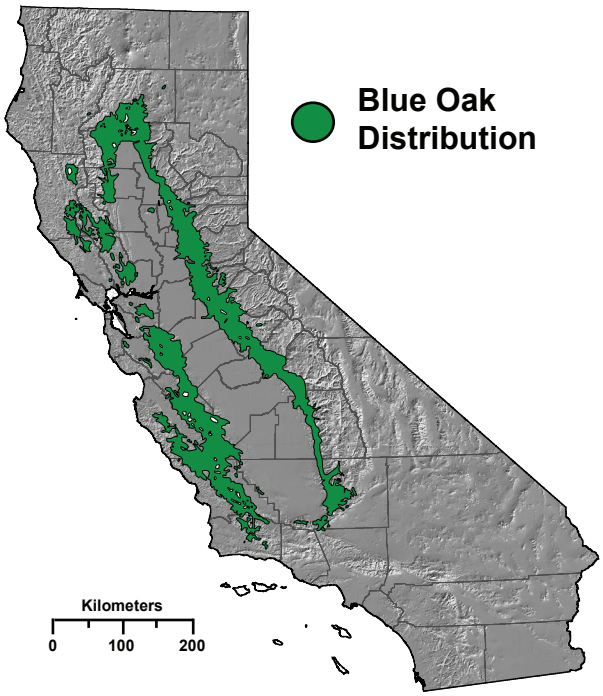

Figure 3 The native distribution of blue oak encircles the Central Valley of California (Griffin and Critchfield 1972) and covers a significant fraction of the San Francisco Bay drainage basin.

water and prevent saltwater intrusion, and the regulation of flow into the estuary for waste water and ecosystem management (Kimmerer and others 2005). Long instrumental, documentary, and proxy records of habitat quality can provide an important perspective on interannual-to-decadal fluctuations in hydroclimatic variables such as precipitation, streamflow, and estuarine salinity. However, variations in the geographical position of the LSZ have been affected by water regulation and by changes in the geometry and bathymetry of the Sacramento–San Joaquin Delta estuarine system, beginning in earnest with hydraulic mining during the Gold Rush. How modern variations in the LSZ might mimic pre-settlement variability cannot be determined with the tree-ring reconstructions developed in this paper because they have been calibrated with LSZ observations made long after the major anthropogenic changes were in place. Instead, the reconstruction of the LSZ presented below provides an estimate for variability in the salinity gradient on interannual-to-decadal time scales, given the present land cover, stream morphology, and regulated flow environment, in response to the range of modern and prehistoric seasonal precipitation totals registered in the tree-ring record over the past 625 years.

These reconstructions are also based on the position of the salinity gradient during the winter, spring, and early summer (i.e., the February–June mean position), and do not extend into the mid- to late-summer period of seasonal drought when landward positions of the LSZ can negatively affect the aquatic ecosystem and Delta agriculture. Nevertheless, the reconstruction provides sensitive centuries-long estimates for how the LSZ would respond to precipitation forcing during the winter–spring–early summer season under the modern realities of this human-altered estuary. There is also strong persistence in the instrumental LSZ data from late spring into late summer, in part because cool-season precipitation totals pre-condition runoff and estuarine water quality during full summer.

The reconstruction of LSZ position based on precipitation-sensitive blue oak chronologies allows us to examine the return intervals between single-year LSZ extrema, and to quantify the frequency of consecutive seasonal maxima and minima in LSZ position over the past 625 years. This provides some empirical expectation for the likelihood of consecutive February–June extremes in the future. These extended estimates of LSZ position during the late 19th and 20th century periods of instrumental sea surface temperature measurements also permit exploration of the potential role of large-scale ocean–atmospheric forcing of the salinity gradient in the estuary.

DATA

Low Salinity Zone

An index of isohaline position was developed by Jassby and others (1995) and is the mean position in the northern arm of the estuary, where the near bottom salinity average is 2‰. The position is measured in kilometers up the northern axis of the estuary from the Golden Gate. The LSZ intrudes landward during the summer dry season and during drought, and

is forced seaward during the winter wet season and years of above-average precipitation and stream flow. There is a systematic relationship between surface and bottom salinity in the northern estuary, so the near bottom position of the 2‰ salinity value was located on the basis of the 1.76‰ surface salinity position (Jassby and others 1995). Missing daily values were estimated from the preceding daily values of isohaline position, river outflow from the Delta (in cubic meters per second), and autoregressive time series modeling techniques (Jassby and others 1995). The daily isohaline data were obtained from A. Jassby (University of California, Davis, pers. comm.) and were then averaged by month (referred to from here as the low salinity zone, or LSZ). The monthly LSZ data were then correlated with the available blue oak chronologies over the water year to determine the optimal season for reconstruction.

Tree-Ring Chronologies

The natural distribution of blue oak nearly encircles the great Central Valley of California, and covers a significant fraction of San Francisco Bay's drainage basin (Figure 3). Blue oak is also referred to as foothills oak and in pre-settlement times it formed the lower forest border with the grasslands of the Central Valley. The upper elevation limit of blue oak woodlands extends into the mixed conifer zone to approximately 5,000 feet. Blue oak trees can achieve impressive size, but they often exhibit an open growth form with little clear stem and, consequently, were not preferred for logging and lumber production (Figure 2). Blue oak woodlands have been extensively cleared for grazing, viticulture, and suburban development, but ancient trees of pre-settlement age survive widely across the more rugged and remote terrain of the Coast Ranges and the foothills of the Cascades and Sierra Nevada. Most of these ancient blue oak woodlands have been affected by grazing, but field surveys indicate that literally millions of canopy blue oak in the 200-year age class still survive across the native range. Individual blue oak over 300 years old are often found in these remnant stands, and trees over 400 years old are occasionally found.

Tree-ring collections were obtained from 36 blue oak woodlands that span the natural distribution of the species (Figure 4), to help document natural hydroclimatic variability across San Francisco Bay's drainage basin (Meko and others 2010). These collections included increment core samples extracted non-destructively from living trees and cross sections cut from the dead wood that sometimes litter these old-growth oak woodlands. At least 40 trees per site were sampled; the average sample size of trees and dead stems was 65 per collection site. The collections were mounted and polished; the growth rings on every specimen were dated to the exact calendar year of ring formation under the microscope using the skeleton plot and visual methods of cross-dating (Douglass 1941; Stokes and Smiley 1995). The mean ring width of the blue oak trees in our sample from 36 sites was only 0.53 mm (based on 2,495 dated trees, for a diameter expansion rate of only 1.06 mm

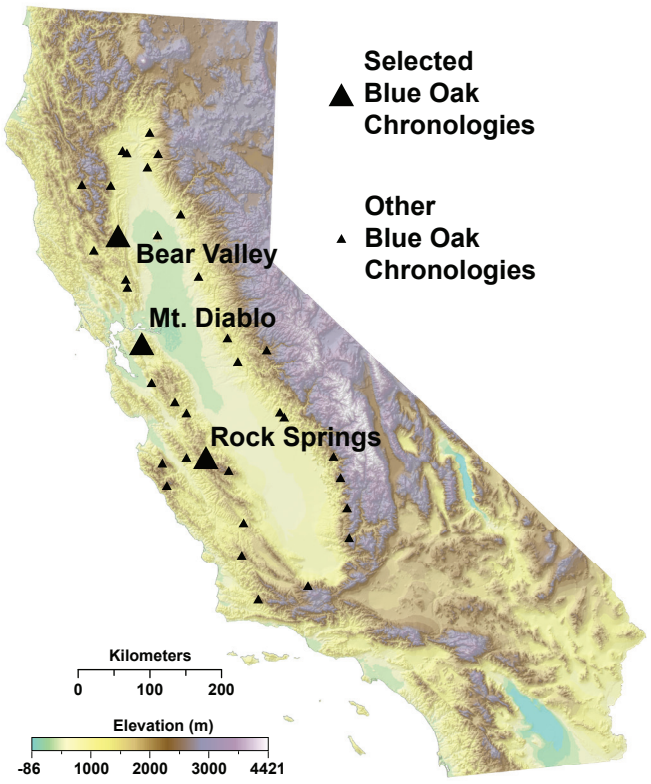

Figure 4 Locations of the 36 blue oak chronologies (all triangles) developed for hydroclimatic study in California. Three blue oak chronologies (large labeled triangles) were used for reconstruction of the LSZ. The digital elevation model for California was obtained from the USGS National Digital Library.

per year). Growth rings were not formed on some trees during certain years of extreme drought (e.g., 1580, 1635) but these "missing rings" were positively identified through crossdating of the highly detailed patterns of wide and narrow rings by comparison with other trees at the site and other sites in the region, which reflects the shared climate history in common to all trees in California.

METHODS

We used the computer program COFECHA (Holmes 1985; Grissino–Mayer 2004) for quality control over the dating and measurement accuracy of all dated radii. We used the program ARSTAN (Cook 1985; Cook and Krusic 2008) to calculate of the mean ring-width chronologies at the three sample locations. Ring-width growth in blue oak is non-stationary in the mean and variance, and mean ring width tends to decline with the increasing size and age of the tree (Figure 5). By fitting empirical growth curves to the raw ring-width time series, we removed this non-climatic growth trend. We calculated ring width indices for each specimen by dividing the ring-width value by the value of the fitted curve for each year. The resulting ring-width indices have a mean of approximately 1.0 for each specimen and a robust mean value function was used to compute the mean index chronology for each collection site (Cook 1985).We used Box–Jenkins time series techniques (Box and Jenkins 1976; Cook 1985) to model and remove low-order persistence in the blue oak ring-width time series believed to be the result of biological memory unrelated to the inter-annual variability of precipitation or related variables such as streamflow or the estuarine position of the salinity gradient. The resulting "residual" ring-width index chronologies resemble a white noise process in the time domain, similar

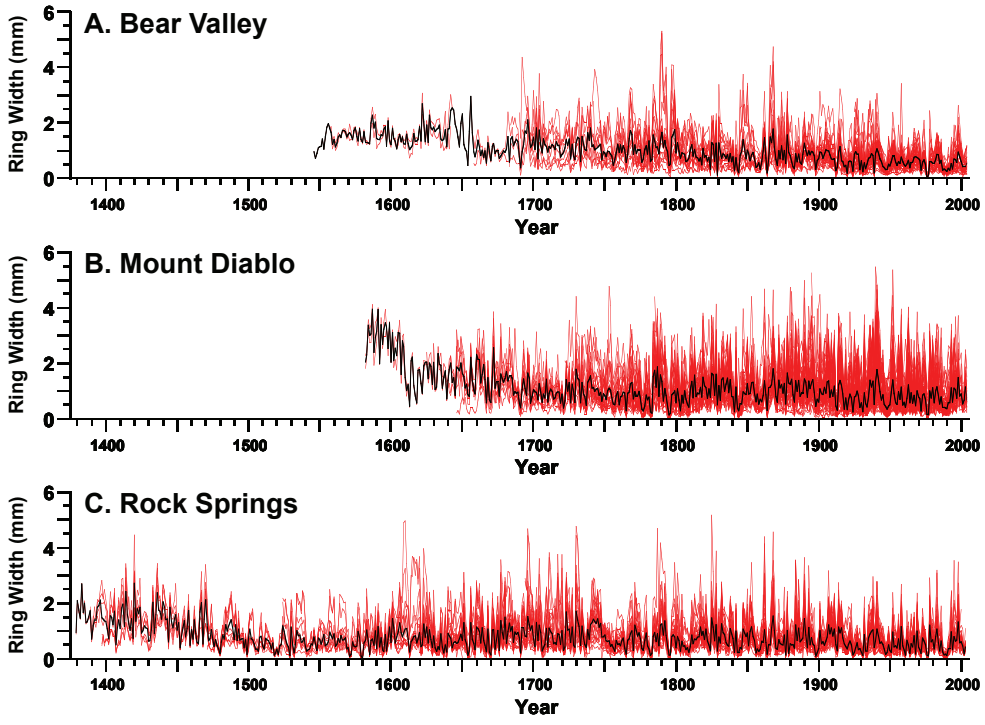

Figure 5 The raw ring widths are plotted for each dated series from the three sites used for LSZ reconstruction (without any detrending or standardization, red time series). The robust mean ring width (discounting outliers, in mm) is illustrated by the black time series for each location (Cook 1985). Note the long-term decline in mean ring width (especially during the first half of each chronology), and the local changes in average variance that are believed to largely reflect biological changes associated with the increasing size and age of the sample trees. The high-frequency variability superimposed on the long-term changes in mean ring width is largely the result of winter–spring precipitation changes over California.

to the seasonal index of the LSZ used for reconstruction.

We screened the 36 available blue oak tree-ring chronologies from California for correlation with the seasonal LSZ data, and selected three long chronologies with high correlations for further analysis, one each from the north, central, and south Coast Ranges (Figure 4). These chronologies were obtained from public and private property at Bear Valley Buttes, Mt. Diablo, and Rock Springs Mountain; they are exceptionally sensitive to seasonal precipitation totals and span a large fraction of San Francisco Bay's drainage basin (Figure 6). The residual chronologies from these three sites were used to compute a regional average chronology, after each chronology was normalized to assure that they would contribute with equal weight to the regional average.

We correlated the regional chronology average with monthly LSZ data to identify the best season for reconstruction. We then averaged the monthly LSZ data for the optimal season (which was determined to be February–June). The lag-1 autocorrelation in the seasonalized LSZ data (February–June) was only $r_{-1} = 0.20$ ($P = 0.18$), and autoregressive modeling did not identify any significant persistence in these seasonalized data available from 1956–2003 (AR = 0). Because we did not find significant low-order persistence in the instrumental LSZ data, we used serially random tree-ring chronologies (AR = 0) in the reconstruction of the seasonal LSZ.

Double mass analysis (Kohler 1949) was used to evaluate the internal homogeneity of both the seasonal LSZ data and the regional blue oak chronology. Double mass analysis involves plotting the simultaneous accumulation of two physically linked variables such as nearby rain gauge records. It is used to identify systematic changes in mean amounts or variance (i.e., inhomogeneities) that can arise from physical changes in the environment surrounding a rain gauge (e.g., growth of overhanging trees or nearby buildings). In the case of streamflow records, anthropogenic diversions for irrigation or municipal supplies, and changes in the geometry of the stream channel near a gauge from upstream construction or land clearing, can introduce inhomogeneities into the

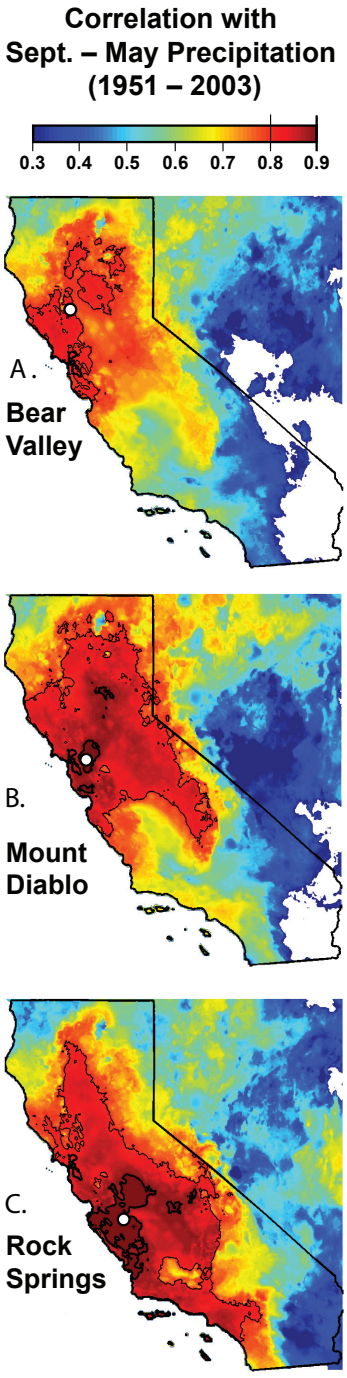

Figure 6 The tree-ring chronologies from Bear Valley Buttes (**A**), Mt. Diablo (**B**), and Rock Springs Mountain (**C**) were each correlated with the seasonal precipitation totals accumulated from September through May at each grid point in the PRISM precipitation data set (PRISM = Parameter-elevation-Regressions-on-Independent-Slopes-Model; Daly and others 2008). The PRISM grid spacing is 4-by-4 km, and has been distributed across the landscape taking into account orographic and topographic effects on precipitation. Correlation coefficients computed between the tree-ring chronologies (indicated by the white dots) and the precipitation data at each grid point are contoured and color-coded. The highest correlations are shown in dark red. Correlations above 0.80 are mapped with the light contour line, correlations above 0.90 with the heavy line. Note the strong and spatially distributed seasonal precipitation signal recorded by these three chronologies (the area with correlations above 0.70), which together cover most of the San Francisco Bay drainage basin.

record. Regional precipitation data (or even tree-ring chronologies) are useful as comparison variables with precipitation, streamflow, or derived hydroclimatic variables, such as the LSZ.

The regional blue oak chronology was submitted to forward stepwise regression to identify potential predictors of seasonal LSZ position. Lead and lag variables derived from the regional chronology were included as potential predictors (i.e., year t_{-1}, t, t_{+1}, t_{+2}) of LSZ position in year t. In all cases reported below, we selected a simple bivariate model based solely on tree growth in year t. We then used the regression coefficients to construct a transfer function to estimate LSZ position based on the value of the regional blue oak chronology. We developed a second experimental reconstruction, based on a sub-period of the available LSZ indices, to test the performance of the blue oak reconstructions when compared with independent LSZ data not used in the calibration. We computed a suite of verification statistics between the estimated and observed LSZ data outside of the calibration period (Fritts 1976; Cook and Kariukstis 1990), and used the general linear model to test for significant differences between the regression coefficients calculated from the full and sub-period calibration models (i.e., full = 1956–2003, sub-period = 1956–1976).

The three-site regional average extends from 1582 to 2003, but the Rock Springs chronology extends from 1379 to 2003, and is highly correlated with monthly and seasonal LSZ position. Therefore, we used the single chronology from Rock Springs to develop a nested reconstruction extending from 1581 back to 1379, with the same forward stepwise regression method used for the full three-site reconstruction outlined above. The normalized residual chronology from Rock Springs was first scaled to equal the variance of the three-site average chronology (i.e., anomalies computed from the Rock Springs chronology by subtracting the mean were multiplied by the ratio of standard deviations calculated for the two chronologies for the 1582–2003 common period, and the mean was then added back to complete the variance equalization). We then added the reconstruction derived from the Rock Springs chronology to the inside of the three-site reconstruction (1379–1581 = Rock Springs only, 1582–2003 = three-site average reconstruction). The variance lost in regression was added back separately for each nested reconstruction into the annual estimates of LSZ position from 1379 to 2003 to complete the continuous 625-year-long reconstruction.

We used return time analysis (Viessman and others 1972) to estimate the recurrence probabilities for single-year LSZ positions of various magnitude during the instrumental (1956–2003) and longer reconstructed time periods. We also tallied the number of consecutive two-year events when the reconstructed LSZ exceeded 110% of the median or fell below 90% of the median: the frequency of these consecutive extrema were plotted against return interval (in years). We examined the large-scale ocean–atmospheric influences on the interannual variability of seasonal LSZ position during the 20th century (1900–2003) with correlation and composite analyses of the global sea surface temperature field during wet (seaward) and dry (landward) extremes of the reconstruction. We investigated low frequency variance in the seasonal LSZ reconstruction over the entire 625-year period, potentially linked with ocean–atmospheric forcing, with spectral (Jenkins and Watts 1968) and wavelet analyses (Torrence and Compo 1995).

RESULTS

The three selected blue oak tree-ring chronologies provide exceptional proxies of seasonal precipitation over a large fraction of San Francisco Bay's drainage basin. The Bear Valley Buttes, Mt. Diablo, and Rock Springs Mountain chronologies were each correlated with September–May precipitation totals at each grid point in the 4-by-4 km PRISM precipitation data set (Daly and others 2008). The strongest correlations with seasonal precipitation ($r \geq 0.90$) were computed with the Mt. Diablo and Rock Springs chronologies, but the spatial correlation pattern of these three chronologies covers most of the region that contributes runoff to San Francisco Bay (Figure 6). These correlation patterns reflect, in part, the organized storms that deliver most of the winter–spring precipitation across California and Nevada. The outstanding regional precipitation history recorded by blue oak chronologies has already been used in the

reconstruction of Sacramento River flow (Meko and others 2001), spatial gradients in precipitation across California (Meko and others 2010), and seasonally-averaged surface salinity in San Francisco Bay (Stahle and others 2001). The widespread precipitation signal illustrated in Figure 6 indicates that blue oak chronologies can be used to estimate the seasonally averaged position of the LSZ under the present land use and water regulations in place for San Francisco Bay's drainage basin.

The monthly LSZ data from 1956 to 2005 are plotted in Figure 7 and illustrate the strong seasonal cycle driven by the Mediterranean precipitation regime of California. The intense two-year drought of 1976–1977 and the six-year drought from 1987–1992 severely depressed California precipitation, reduced Sacramento–San Joaquin stream flow, and had a major affect on the longitudinal salinity gradient. The seasonal LSZ maxima in 1959, 1960, and 1961 all occurred during dry years in California, but these years were not nearly so dry as 1976–1977. These three maxima all occurred after the February–June season used for reconstruction, and may have been aggravated by artificial water withdrawal from the Delta. The wet conditions during the 1982–1983 El Niño were associated with the most seaward position of the LSZ during the instrumental period (Figures 1 and 7; Jassby and others 1995).

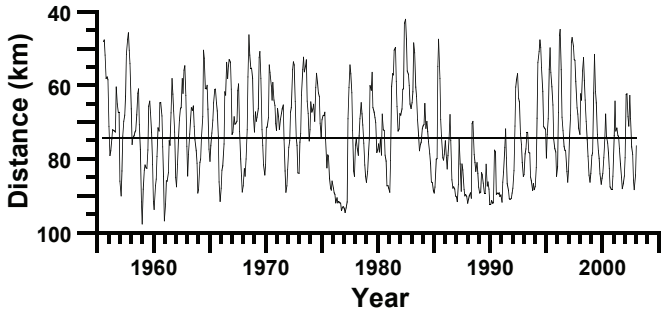

Figure 7 Monthly LSZ means (based on daily data from Jassby and others 1995) are plotted from October 1, 1956 to September 30, 2005. The y-axis has been inverted here and in Figures 10 and 11 so that drought years with low flow and a landward position of the LSZ are plotted below the mean. Note the droughts and LSZ maxima during 1976–1977 and 1987–1995. The LSZ minima occurred during the El Niño event of 1983.

The average monthly positions of the LSZ are plotted by water year in Figure 8A, and illustrate the strong seasonal minima during the winter–spring period of high precipitation and runoff, which forces the salt field seaward. The mean March position is located within Suisun Bay; the mean August position is near the lower Delta (62.3 and 81.9 km, respectively;

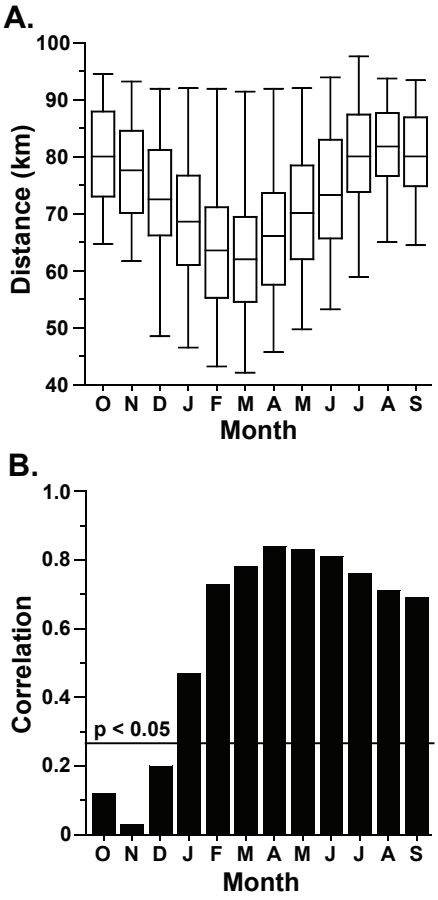

Figure 8 **(A)** Box plots of the monthly LSZ indices calculated from instrumental and model data by Jassby and others (1995) from 1956–2003 are illustrated for the water year (mean = horizontal bar; the 25th and 75th percentiles are within the box; the monthly maximum and minimum positions are at the whiskers; data truncated to 2003 to match the end date of the tree-ring data). **(B)** The correlation coefficients computed between the monthly LSZ indices and the regional blue oak tree-ring chronology (the tree-ring chronology in year t was correlated with January–September LSZ index also in year t, but with October–December LSZ indices in year t_{-1}). The correlations exceed $P < 0.05$ from January-September.

Figures 1 and 8A). To define the best LSZ season for reconstruction with the tree-ring data, the regional blue oak chronology was correlated with the monthly LSZ index for the period from 1956 to 2003. The tree-ring data are significantly correlated with the LSZ position for 9 of 12 months, and the correlations exceed $r = 0.70$ from February through June (Figure 8B). We chose the period from February–June as the optimal period for reconstruction and averaged the instrumental LSZ data for these five months. The regional blue oak chronology is correlated with the February–June LSZ index at $r = 0.86$ for the 1956–2003 period, which reflects the strong biogeophysical coupling between California precipitation, blue oak growth, streamflow, and the geographical position of the salinity gradient in the estuary. (Note that the individual chronologies are also well correlated with the February–June LSZ position from 1956–2003: Bear Valley Buttes = 0.80, Mt. Diablo = 0.83, and Rock Springs = 0.78).

In spite of the high correlations between the regional tree ring chronology and the salinity gradient, double mass analysis indicates that the seasonal LSZ data were subject to persistent excursions from regional precipitation forcing near the time of the two worst droughts during the late 20th century (i.e., 1977 and 1986, Figure 9). Double mass analyses were performed on seasonal precipitation averaged for climate divisions 2 and 5 in central California (Karl and others 1983), the regional blue oak chronology, the seasonal LSZ data, and the seasonal Delta outflow used in the computation of the LSZ index (e.g., CDWR 1999; Knowles 2002). The double mass plot between regional precipitation and the regional tree-ring chronology does not indicate any discontinuities between the two accumulations (Figure 9A), which suggests that both variables are internally homogeneous. However, the comparison between the precipitation and the seasonal LSZ index indicates modest excursions in the LSZ data starting at approximately 1977 and 1986 (Figure 9B). Similar results were observed for the comparison between the regional tree-ring chronology and the LSZ data (Figure 9C). The double mass plot comparing seasonal Delta outflow with the seasonal precipitation data also indicates persistent excursions beginning at approximately 1977 and

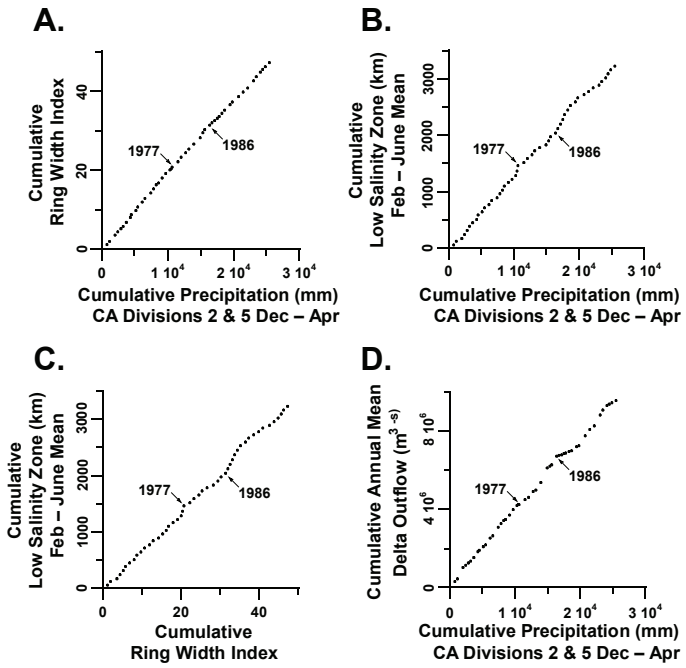

Figure 9 Double mass analyses of precipitation, ring width, LSZ position, and Delta outflow are illustrated. (**A**) Cumulative precipitation and ring width indices are plotted for the period from 1956–2003. The first dot near the origin for all panels represents 1956, the last dot in the top represents 2003. Cumulative precipitation and LSZ position are plotted in (**B**); cumulative ring width and LSZ position in (**C**), and cumulative precipitation and Delta outflow from the Sacramento and San Joaquin rivers in (**D**). Note the apparent discontinuities at 1977 and 1986 in the comparisons between precipitation/ring width and LSZ/Delta outflow in Figures 9B, 9C, and 9D.

1986 (Figure 9D). Note that accumulated outflow increases more slowly than accumulated precipitation (Figure 9D), which implies less Delta outflow per unit of precipitation during these two drought regimes. This could reflect a natural and/or managerial effect (e.g., withholding water during drought), but it led to accumulated LSZ positions rising more rapidly than either accumulated precipitation or ring width during these same drought episodes (Figures 9B and 9C, respectively). These results suggest that the LSZ index and Delta outflow estimates are not entirely free of non-climatic effects associated with the droughts of 1976–1977 and 1987–1992. The persistent excursions between the tree ring and LSZ data beginning in 1977 and 1986 are not large (Figure 9B), but they

have affected the residuals from the regression model that links the two variables (see discussion below).

The regional tree-ring chronology was separated into four potential predictors of the February–June salinity gradient with years t_{-1}, t, t_{+1}, t_{+2} and submitted to forward stepwise regression. Blue oak growth in year t provided the best predictor, and the lead and lag variables did not significantly improve the regression model. The bivariate regression model used to estimate LSZ position was

$$\hat{Y}_t = 67.367 - 9.646X_t \quad (1)$$

where $\hat{Y}_t$ is the estimated LSZ position in year t, and X_t is the regional tree-ring chronology also in year t. The relationship between the estimated and actual values of the February–June LSZ index during the calibration period 1956–2003 is summarized in Table 1 and illustrated in Figures 10A and 10B. The regional tree-ring chronology provides a good estimate of the actual data (R^2 adjusted = 0.73), particularly considering that this model is based entirely on the orchestration of tree growth, runoff, and LSZ variability by large-scale precipitation across a drainage basin that covers 165,700 km^2. The tree-ring chronology under-estimates the observed data from 1987–1992 during the most persistent drought of the instrumental period, and over-estimates the LSZ position during three wet years (1978, 1993, and 1998; Figure 10B). The persistent under-estimation may result, in part, from water export from the Delta during this drought, and has led to significant autocorrelation in the regression residuals and a poor Durbin–Watson statistic (Table 1). The inclusion of additional lagged predictors in the forward stepwise regression modeling, including a quadratic transformation of the tree-ring data, did not eliminate this problem. When the regression was based on the period from 1956 to 1976, before the apparent inhomogeneity in the LSZ data, the tree-ring chronology accounted for 85% of the variance, and had no significant autocorrelation in the regression residuals. The LSZ estimates derived from this short calibration period passed most of the verification tests when compared with statistically independent instrumental data available from 1977 to 2003 (Table 2). But because the shorter calibration period excluded the most extreme minima and maxima in LSZ position, we choose to use the full calibration period model, which explained 73% of the variance from 1956 to 2003 for reconstruction in order to better estimate the frequency of LSZ minima and maxima over the past 625 years. The results presented in Table 1 indicate that the blue oak chronologies provide good estimates of the high frequency precipitation-driven variance in the salinity gradient, in spite of the modest inhomogeneity in the instrumental LSZ indices and the poor Durbin–Watson statistic (Figure 9, Table 1).

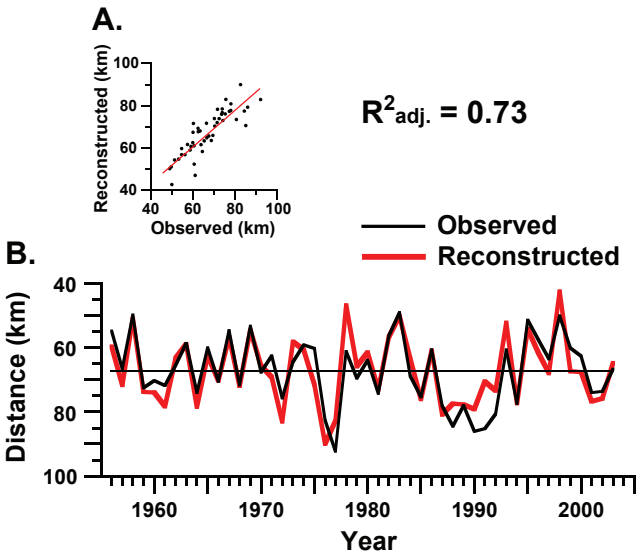

Figure 10 The tree-ring data were calibrated with the February–June average LSZ position from 1956 to 2003. The instrumental and reconstructed LSZ locations are compared in a scatter plot (**A**) and a time series plot (**B**). The tree-ring data explain 73.0% of the variance in the LSZ data, but underestimate the severity of the 1987–1992 drought/LSZ maxima, which may reflect both persistent drought and water export from the Delta.

The reconstructed seasonal LSZ locations are plotted from AD 1379 to 2003 in Figure 11, along with two smoothed versions emphasizing five- and ten-year variability. The instrumental and reconstructed LSZ indices for the February–June season are tabulated in Tables 3 and 4. The reconstructed LSZ data range from a minimum of 37.7 to a maximum of 90.0 km, and the highest single year maxima in the entire reconstruction occurred in 1976. In fact,

Table 1 Calibration statistics computed for the two regression estimates of the position of the February–June LSZ based on the three-site and single-site tree-ring chronologies. The variance lost in regression was restored to all 625 reconstructed values using the ratio of the observed and reconstructed standard deviations in the calibration period (10.467/8.785 = 1.191). The statistics calculated for the calibration period were the R^2 adjusted for loss of degrees of freedom, the root mean squared error (RMSE), and the Durbin–Watson statistic (DW) that tests for autocorrelation in the residuals from the regression model (Draper and Smith 1981). The autocorrelation in the residuals was r_{-1} = 0.44 and 0.47 for the three-site and single-site calibrations, which are both significant according to the DW test at $P < 0.05$.

	Time Period	b_0	b_1	R^2adj.	RMSE	DW
Three-Site Calibration	1956–2003	67.367	–9.646	0.733	5.407	1.092
Single-Site Calibration	1956–2003	67.369	–7.756	0.606	6.572	1.036

Table 2 A verification experiment was performed using the 1956–1976 subperiod. A calibration based on the 1956–1976 period was verified by comparison with the instrumental LSZ data available from 1977–2003. The statistics calculated for the verification period are the Pearson correlation coefficient (r), correlation of first-differenced series, paired t-test, reduction of error (RE) and the coefficient of efficiency (CE). The experimental subperiod reconstruction passed all of the statistical tests in the verification period except for the test of the mean. (See Cook and Kairiukstis 1990 for further details on the verification statistics.)

	1956–1976	1977–2003
Correlation (r)	0.91 ($P < 0.0001$)	0.85 ($P < 0.001$)
First-Difference Correlation	0.91 ($P < 0.0001$)	0.89 ($P < 0.0001$)
***t*-test for Difference of Mean**	0.00 (ns)	4.54 km (0.001)
Reduction of Error	---	0.60
Coefficient of Efficiency	---	0.56

the reconstruction indicates that some of the most extreme single-year, two-year, five-year, and ten-year droughts and LSZ maxima occurred during the 20th century (Table 4). The worst two-year drought/LSZ extreme was reconstructed for 1976–1977, and the most persistent decadal episode was reconstructed from 1917 to 1934 (Figure 11). The most extreme reconstructed wet years with LSZ minima during the 20th century occurred during the El Niño years of 1998, 1983, 1978, 1958, and 1941, but these wet years may have been exceeded by six LSZ minima during the preceding five centuries (Figure 11).

Return time analyses were used to estimate the probability of single-year LSZ minima and maxima. We also used return time analysis to compare the instrumental LSZ data from 1956 to 2003 with the tree ring reconstructed estimates during the presettlement period from 1582 to 1850 (when the reconstruction is well replicated, Figures 11D and 12). The recurrence probabilities for LSZ maxima and minima ≥1.0 standard deviations from the mean are nearly identical for the two periods (Figure 12). The recurrence probabilities for maxima ≥1.75 standard deviations above the mean were slightly higher during the 48 years from 1956 to 2003 than during the presettlement era (i.e., a 50% return probability at every 17.0 years compared with every 19.0 years from 1582 to 1850). These results indicate little difference in the probability of LSZ maxima and minima during the presettlement era compared with the instrumental period, and suggest that the variability in the LSZ that arises strictly from cool-season precipitation fluctuations, and as recorded by blue oak trees, has not dramatically changed from 1582–2003. How the seasonal position of the LSZ might have migrated under fully natural conditions before human development of the drainage basin and estuary remains an open question, which might be addressed with analyses of estuarine sediments and other proxies (Starratt 2007; Malamud–Roam and others 2007).

These results that compare hydroclimatic variability during the 20th century with the preceding 500

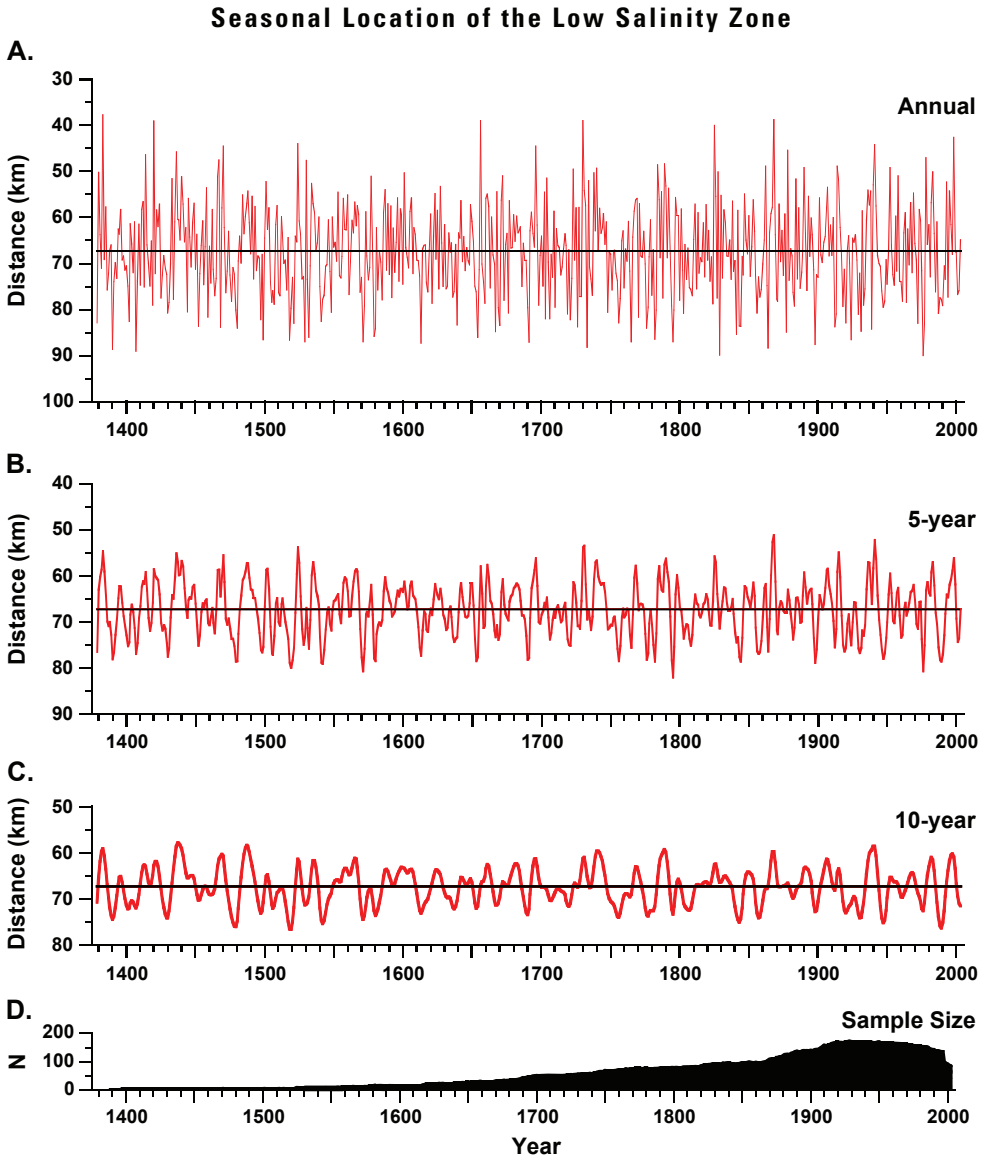

Figure 11 The tree-ring reconstructed February–June LSZ locations are plotted on an annual basis from 1379 to 2003 in (A), with 5-year smoothing in (B), and with 10-year smoothing in (C; note that the y-axis is inverted in A–C so that "dry" LSZ maxima are below mean and "wet" minima are above mean). The sample size of dated blue oak series is plotted in (D, for individual radii). The best-replicated period begins in 1582, when 30 radii from all three sites become available. Note the extreme LSZ maxima estimated for 1976 (A), the unusual 6-year run of drought and LSZ maxima from 1987–1992 (A,B,C), and the persistent drought/LSZ maxima from 1917–1934 (C).

Table 3 Instrumental February–June average LSZ position listed in kilometers from the Golden Gate (Source: Jassby and others 1995).

Date	0	1	2	3	4	5	6	7	8	9
1956	---	---	---	---	---	---	54.78	66.54	49.88	72.56
1960	70.32	71.82	65.52	58.74	74.06	60.14	70.52	54.72	71.62	53.36
1970	67.72	62.58	75.74	64.60	59.20	60.36	82.68	92.22	61.24	69.60
1980	63.96	74.30	56.42	49.16	68.82	75.44	60.70	78.18	84.48	78.08
1990	86.12	85.24	80.70	60.74	77.36	51.44	57.52	63.58	50.18	60.20
2000	62.68	74.02	73.70	66.72	---	---	---	---	---	---

Table 4 Tree-ring reconstructed February–June seasonal LSZ position listed in kilometers from the Golden Gate.

Date	0	1	2	3	4	5	6	7	8	9
1379	—	—	—	—	—	—	—	—	—	82.95
1380	50.20	63.73	71.04	37.71	69.15	57.72	75.78	72.11	67.34	65.96
1390	88.71	74.00	69.79	73.25	62.47	63.63	58.26	69.32	68.30	71.47
1400	70.50	74.86	82.65	61.43	65.74	72.00	60.91	89.07	73.77	61.47
1410	74.67	58.19	56.58	75.10	46.37	65.92	70.05	74.96	65.08	79.05
1420	39.08	72.23	58.33	61.96	57.14	77.50	72.56	68.20	71.04	72.35
1430	80.76	78.48	70.09	51.60	77.82	61.00	45.73	60.39	60.56	64.89
1440	51.10	57.05	65.36	62.19	80.57	55.81	64.29	70.72	61.17	56.88
1450	71.23	63.68	83.67	72.23	66.06	60.68	74.66	66.36	53.57	81.74
1460	66.27	74.33	58.21	71.23	76.99	73.21	51.10	47.46	83.88	57.95
1470	44.47	62.24	76.40	71.70	63.11	72.56	78.20	70.90	72.28	80.11
1480	84.02	69.44	64.03	69.86	55.16	63.56	59.82	56.88	54.34	61.12
1490	67.90	55.46	73.30	57.65	71.54	68.32	68.93	82.22	68.04	86.60
1500	64.55	52.27	62.59	57.93	74.00	78.45	75.85	78.85	61.57	57.40
1510	76.24	77.01	59.84	63.35	70.02	69.29	75.73	64.41	86.63	79.69
1520	73.10	83.00	64.10	65.29	44.00	60.72	63.61	73.37	72.86	86.98
1530	47.65	73.49	86.03	70.53	52.67	57.00	59.04	67.23	65.55	59.86
1540	75.03	82.69	77.84	76.87	70.62	70.25	60.58	71.75	80.64	59.96
1550	66.48	65.48	69.44	54.44	72.58	73.12	68.48	55.91	62.59	62.75
1560	55.16	76.80	69.69	60.65	63.38	56.74	61.77	57.42	59.42	76.28
1570	73.07	86.98	79.15	58.80	68.41	73.58	70.88	51.03	66.04	85.84
1580	84.07	62.24	75.74	67.24	69.67	77.91	58.97	54.02	71.48	56.99
1590	72.35	57.48	77.45	62.30	71.91	65.44	55.78	73.85	58.16	59.39
1600	74.47	50.27	66.56	68.61	71.01	58.75	55.70	72.27	62.26	63.62
1610	69.32	69.40	72.73	87.33	66.89	66.08	65.99	74.02	76.15	67.02
1620	59.29	78.62	64.08	54.84	69.04	58.45	75.52	53.26	65.56	74.97
1630	61.61	75.59	74.88	63.41	67.56	65.49	77.29	76.08	65.81	83.32
1640	63.32	64.50	56.39	69.62	64.18	71.60	66.57	69.39	70.28	57.24
1650	60.87	65.34	74.92	76.18	86.07	71.42	38.99	70.15	74.03	78.71
1660	55.80	54.88	57.65	75.28	59.96	68.14	70.25	84.79	54.39	79.61
1670	83.44	56.22	51.00	78.06	65.87	63.44	80.74	56.41	66.64	66.54
1680	59.37	65.26	59.68	63.36	62.76	61.98	75.02	65.67	69.31	69.25
1690	79.57	87.06	62.93	58.91	63.46	66.45	44.49	61.73	79.10	68.28
1700	64.05	74.92	54.52	82.01	51.46	69.77	81.94	68.01	73.09	58.64
1710	79.53	62.42	66.09	66.54	72.48	70.79	66.77	63.56	66.05	80.93
1720	67.03	82.26	73.23	49.44	69.29	57.91	83.80	57.86	77.20	77.17
1730	38.99	54.18	57.36	88.27	51.97	70.70	73.36	76.90	50.37	62.91
1740	49.34	67.37	58.04	63.51	62.24	59.24	65.86	60.93	80.63	67.47
1750	68.08	75.68	67.46	67.12	72.07	73.81	82.91	77.62	65.11	62.93
1760	75.35	66.87	69.44	60.85	71.68	87.05	64.30	58.65	56.31	55.85
1770	81.72	56.94	68.37	68.60	63.01	70.18	84.02	79.52	68.56	60.51
1780	76.92	66.94	86.51	80.18	48.58	56.13	68.82	54.42	77.47	48.40
1790	53.12	68.73	53.63	67.89	79.16	86.99	80.15	55.67	59.60	59.61
1800	78.06	58.12	71.48	80.81	65.91	73.48	66.73	75.20	75.63	77.05
1810	64.81	57.12	75.52	59.01	72.13	68.79	69.55	61.18	72.91	57.26
1820	69.35	62.87	73.91	68.56	78.75	40.01	55.42	77.48	50.13	89.90
1830	55.25	73.15	58.40	61.17	68.40	68.47	64.93	73.51	56.47	71.78
1840	69.37	85.39	58.44	83.53	83.62	68.46	72.56	54.86	64.90	67.94
1850	59.56	72.85	66.39	56.14	63.07	72.49	80.71	72.93	77.32	75.66
1860	70.18	64.95	48.84	74.77	88.31	63.38	59.13	57.78	38.81	63.76
1870	77.69	78.30	57.11	69.62	62.86	72.61	59.33	84.85	45.38	73.69
1880	66.85	68.34	76.30	79.27	51.71	73.40	57.90	75.45	71.89	67.29
1890	49.13	63.50	75.86	55.40	68.47	60.11	63.79	71.40	87.64	72.43
1900	72.99	55.79	68.15	69.84	65.41	64.16	57.84	53.50	68.34	61.74
1910	68.22	60.03	83.76	80.93	48.91	51.82	62.27	68.37	79.43	71.22
1920	82.89	67.25	64.00	69.86	86.60	64.51	65.38	63.75	69.28	81.06
1930	72.11	84.70	58.58	79.05	75.57	60.56	54.13	57.28	54.35	84.33
1940	52.89	44.24	57.48	68.28	69.99	70.66	75.93	79.53	78.15	69.17
1950	74.45	67.42	49.20	66.02	72.37	74.75	59.67	71.70	51.02	73.86
1960	73.94	78.27	63.32	58.97	78.44	62.51	70.31	56.77	72.00	54.68
1970	65.64	69.30	82.99	58.25	60.72	71.53	89.99	82.89	46.94	65.89
1980	61.56	72.98	56.76	50.16	63.50	76.11	60.97	80.85	77.45	77.78
1990	79.21	70.59	73.47	52.29	77.29	54.30	61.58	68.01	42.61	67.39
2000	67.68	76.75	75.87	64.79	—	—	—	—	—	—

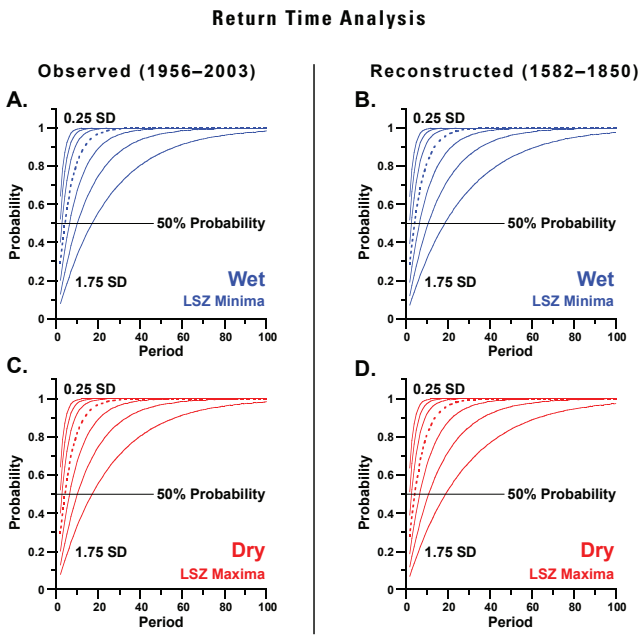

Figure 12 Return time analyses were computed for seven thresholds of observed and reconstructed LSZ position, both above and below the mean (0.25, 0.50, 0.75, 1.0, 1.25, 1.50, and 1.75 standard deviations) and for return periods from 2 to 99 years. The lowest threshold (0.25) is plotted at far left in all panels. Note that the 50% recurrence probability for extremely wet years with a LSZ minima ≥1.75 standard deviations from the mean is 18.1 years, based on the observed data from 1956–2003 (**A**), and 19.1 years for the reconstructed data during the pre-settlement era from 1582–1850 (**B**).

years are similar to the conclusions drawn by Meko and others (2001) for a tree-ring reconstruction of Sacramento River flow, but they contrast with the results of Haston and Michaelson (1994) who found reduced 20th century variability in a tree-ring reconstruction of precipitation for Santa Barbara. Our results also contrast sharply with the reconstruction of more persistent decadal droughts over the Sacramento basin prior to AD 1400 (Meko and others 2001), and with the evidence for extreme changes in the water balance over California during the Medieval Era (Stine 1992; Graham and others 2006). The reconstructed LSZ data do not extend back into the Medieval Era, and the tree-ring reconstruction of hydroclimatic variability can be sensitive to the techniques of chronology development, including the detrending and standardization of ring width time series, regional chronology development and variance stabilization. However, proxy ring-width time series are subject to systematic changes in the mean and variance over the life of the organism and these changes are not related to climate variability (Figure 5). Various ad hoc techniques have been used to recover low-frequency variability from tree ring data. When long-term variability in tree ring data is replicated broadly over space among many different species and forest environments, it is reasonable to conclude that the low-frequency changes arise from climate and not biological causes. The low-frequency changes in the mean and variance in the three chronologies used for this analysis are dominated by age- and size-related trend (mainly in the first half of each chronology, Figure 5), so we choose to concentrate on the high-frequency variability of blue oak growth that can be related unambiguously to precipitation, stream flow, and the resulting position of the LSZ.

Because the environmental impact of LSZ extremes that occur in consecutive years may be more problematic than single-year extrema, the intervals between consecutive reconstructed LSZ extremes were tallied for the past 625 years and the frequency distribution of consecutive seasonal maxima and minima are plotted in Figure 13. Extremes were defined as follows: LSZ maxima ≥110% of the median and minima as ≤90% of the median. The intervals between consecutive two-year extremes were grouped into three-year bins for illustration (Figure 13). There were 16 consecutive "wet" or low LSZ extremes that occurred within one to three years over the past 625 years, which largely reflects the tendency for wet regimes and low LSZ positions to persist for two to five years. Short intervals between consecutive "dry" LSZ regimes were less frequent than consecutive wet regimes based on this arbitrary ±10% threshold analysis of the reconstructed LSZ positions. Nevertheless, the frequency distributions in Figure 13 provide at least a first-order empirical expectation for the likelihood of consecutive February–June extremes in the future.

Jassby and others (1995) noted that the most extreme LSZ minima in the instrumental record occurred during the major El Niño event of 1983, when California

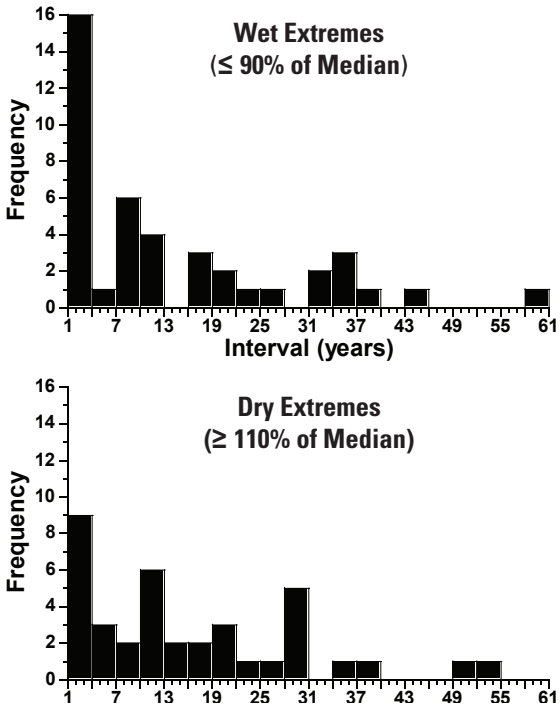

Figure 13 The frequency distribution of intervals between consecutive LSZ extremes is illustrated based on the 625-year reconstruction. Extremes were defined as reconstructed LSZ maxima ≥110% of the median, minima as ≤90% of the median, and the intervals between consecutive 2-year extremes were grouped into 3-year bins for illustration.

was very wet. The reconstructed LSZ data confirm this tendency, and indicate that the lowest minima over the past 150 years have typically occurred during warm El Niño conditions [i.e, nine of the ten lowest LSZ positions occurred in El Niño years [defined simply as a positive bivariate ENSO time series average for the DJFM season from Smith and Sardeshmukh (2000)] (Table 5, Figure 11). Only four of the ten most extreme LSZ maxima occurred during La Nina events (i.e., negative bivariate ENSO indices for DJFM), and six extreme LSZ minima occurred during weak El Niño events (Table 5).

To explore the large-scale ocean–atmospheric features associated with the interannual variability of seasonal LSZ positions, we used correlation and composite analyses of the global SST field for the period 1900–2003 (Kaplan and others 1997). The reconstructed February–June LSZ data were correlated with winter (January–April) SSTs and the classic gradient in SSTs in the north Pacific between Hawaii and the West Coast of North America was identified (Figure 14A). Drought and LSZ maxima are most strongly associated with warm SSTs northeast of Hawaii, and with cold SSTs to the southeast. The SST correlation patterns in Figure 14A are consistent with a strengthened Aleutian low, enhanced meridional flow, and a mean storm track over the Pacific Northwest, leaving most of California relatively dry. Wet winter and spring conditions and LSZ minima are associated with the reverse SST patterns (Figure 14A), which would tend to direct the storm track directly into California.

These correlation analyses do not indicate a prominent association with SST variations over the equatorial Pacific. However, the importance of El Niño conditions is evident when the SSTs are averaged and mapped for the ten years with the most extreme reconstructed LSZ minima (Figure 14B). These wet years over California from 1900 to 2003 have been associated with warm SSTs in the eastern equatorial Pacific and with the warm phase of the Pacific Decadal Oscillation (PDO) in the north Pacific. The SST pattern in Figure 14B is associated with strong convection in the central and eastern equatorial Pacific, a stronger subtropical jet stream, and the advection of moisture and momentum into southwestern North America. At the same time, the SST gradient over the northeast Pacific is weaker. However, the ten most extreme dry years with reconstructed LSZ maxima from 1900 to 2003 were not strongly associated with the opposite La Niña-like SST pattern over the equatorial Pacific (Figure 14C). In fact, central California is located near the wet–dry divide in the average ENSO teleconnection pattern to western North America and, in “normal” El Niño events, the Pacific Northwest tends to be dry. But the strongest El Niño events tend to be linked with the development of wet conditions extensively along the West Coast (Hoerling and Kumar 2000). The composite SST map during the most exceptionally wet LSZ minima conditions appears to have been dominated by the strongest El Niño events of the 20th century (Figure 14B, Table 5).

Spectral analysis (Jenkins and Watts 1968) of the well-replicated reconstruction from 1582 to 2003

Table 5 The most extreme maxima and minima in reconstructed LSZ position for the period 1871–2003 contemporaneous with the bivariate ENSO index of Smith and Sardeshmukh (2000). El Niño conditions during the preceding and current winter are indicated by an E (based on a positive seasonal index average for December–March), La Niña conditions are indicated by L (based a negative seasonal index). The most extreme reconstructed LSZ maxima and minima are also shown for 1379–2003.

Low Salinity Zone Maxima 1876–2003

Rank	Year	Value
1	1976L	89.99
2	1898L	87.64
3	1924E	86.60
4	1877E	84.85
5	1931E	84.70
6	1939L	84.33
7	1912E	83.76
8	1972L	82.99
9	1920E	82.89
10	1977E	82.89

Low Salinity Zone Minima 1876–2003

Rank	Year	Value
1	1998E	42.61
2	1941E	44.24
3	1878E	45.38
4	1978E	46.94
5	1914E	48.91
6	1890L	49.13
7	1952E	49.20
8	1983E	50.16
9	1958E	51.02
10	1884E	51.71

Low Salinity Zone Maxima 1379–2003

Rank	Year	Value
1	1976	89.99
2	1829	89.90
3	1407	89.07
4	1390	88.71
5	1864	88.31
6	1733	88.27
7	1898	87.64
8	1613	87.33
9	1691	87.06
10	1765	87.05

Low Salinity Zone Minima 1379–2003

Rank	Year	Value
1	1383	37.71
2	1868	38.82
3	1656	38.99
4	1730	38.99
5	1420	39.08
6	1825	40.01
7	1998	42.61
8	1524	44.00
9	1941	44.24
10	1470	44.47

indicates weak concentrations of variance at periods near 5, 7, and 15 years (Figure 15A). These spectral peaks are significant at up to the 99% confidence level, but each peak represents no more than 5% of the reconstructed time series variance. Wavelet analysis (Torrence and Compo 1998) further indicates that the concentrations in reconstructed variance in these three frequency bands have been highly episodic over the past 625 years (Figure 15B). LSZ variability in the frequency band nominally referred to as the ENSO band (i.e., with periods centered near 5 years) was prominent only for short intervals (e.g., during the late 15th, mid-17th, and late 20th centuries), and power in this band virtually disappeared during the early 17th and early 19th centuries (Figure 15B). Power in the 15-year frequency band appears to have been important during much of the 20th century, but was largely absent during the 17th and early 18th century (Figure 15B). This particular 15-year frequency component is vaguely apparent in the amplitude of the decadally smoothed reconstruction (Figure 11C, especially in the late 15th and 20th centuries), but is probably not associated with the PDO, which has a longer time scale of variation, typically

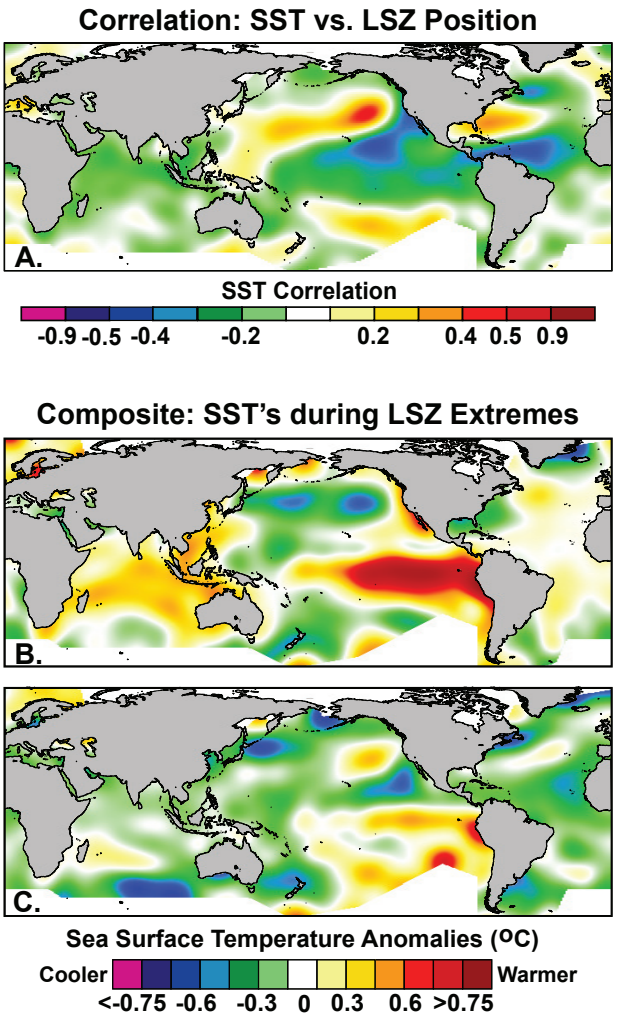

Figure 14 **(A)** The reconstructed February–June LSZ positions were correlated with seasonalized (JFMA) sea surface temperature data from 1900–2003 (from Kaplan and others 1997). Droughts and LSZ maxima are correlated with warm SSTs northeast of Hawaii and cold SSTs to the southeast. Wet conditions and LSZ minima are correlated with the inverse of this SST pattern. **(B)** A composite map of the Kaplan and others (1997) SST data during the ten most extreme reconstructed minima in LSZ position indicates that these wet years are often associated with El Niño conditions in the eastern equatorial Pacific (analyses restricted to the 1900–2003 period). **(C)** The composite map of SSTs during the ten most extreme reconstructed LSZ maxima indicates that forcing from the equatorial Pacific is not as important during droughts over California.

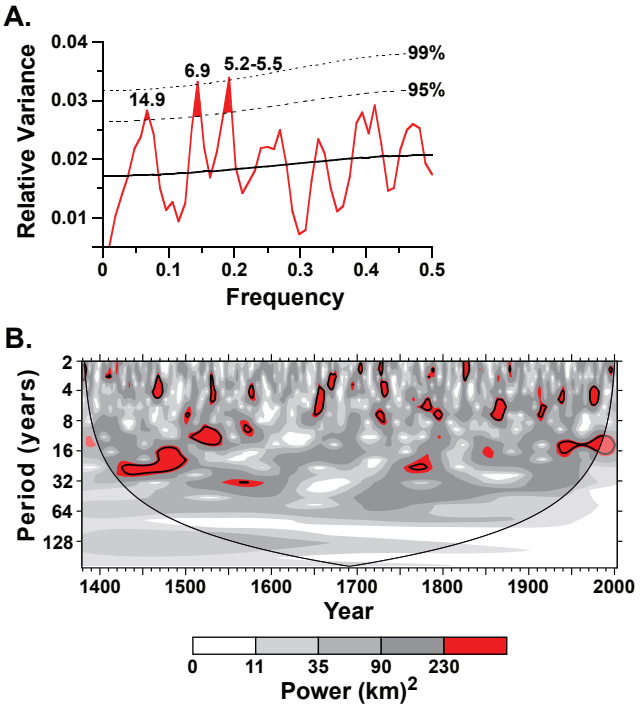

Figure 15 **(A)** The spectral density function calculated on the well-replicated reconstruction of the February–June LSZ position from 1582–2003 has three significant peaks at 5.2 to 5.5, 6.9, and 14.9 years [based on a Hamming window with a bandwidth of 0.0252, 40 degrees of freedom, and 50 lags in estimating the autocorrelation function, tested for significance against a white noise null continuum (IMSL® Inc., 1982)]. **(B)** The time dependence of the low frequency variance in the reconstructed LSZ estimates was examined with wavelet analysis (from: *http://ion.researchsystems.com/cgi-bin/ion-p*), which indicates that variance in the ≈5-, ≈7-, and ≈15-year frequency bands have been highly non-stationary over the past 625 years. (Local wavelet power significant at the 0.05 level is outlined with black contours, tested against a white noise model.) Contour levels for the spectrum pass 75%, 50%, 25%, and 5% of the wavelet power at each level (from left to right). Note that power in the ENSO band (≈5-year) virtually disappeared during the early 17th and 19th centuries in this reconstruction.

25 to 35 years (Zhang and others 1997). This decadal to multi-decadal mode near 15 years has been previously detected in hydroclimatic data from California but has not been conclusively diagnosed.

SUMMARY AND CONCLUSIONS

The following conclusions summarize the rationale and results of this research project:

1. The mean position of the bottom water salinity front, or low salinity zone (LSZ), is strongly correlated with many physical and ecological conditions in the northern reach of San Francisco Bay.
2. The position of the LSZ is tightly coupled with freshwater inflow to the estuary, precipitation over the drainage basin and, ultimately, to regional and large-scale climate variability.
3. Blue oak tree-ring chronologies are sensitive to cool-season precipitation totals across San Francisco Bay's drainage basin, and are also well correlated with seasonal streamflow totals in California, with surface salinity at the Golden Gate, and with the longitudinal salinity gradient in the northern reach of the estuary.
4. The precipitation signal embedded in the proxy blue oak chronologies cannot be used to reconstruct variability in the LSZ under fully natural conditions before water regulation and land use change, but it can be used to estimate the range of seasonal low-salinity positions that might have occurred under the natural climate variability of the past 625 years, given the existing conditions in the estuary: the modern land cover, channel geometry, estuarine bathymetry, and regulated water regime.
5. Three selected blue oak chronologies were used to develop a reconstruction of the February–June average LSZ position from AD 1379 to 2003, explaining 73% of the variance in the instrumental data during the 1956–2003 calibration period.
6. This reconstruction succeeds because the blue oak chronologies faithfully record a significant fraction of winter–spring precipitation totals over San Francisco Bay's drainage basin. The February–June season of reconstruction precedes the late summer dry period when extreme maxima in the salinity field create management concerns for Delta agriculture and aquatic ecosystem function. Nevertheless, the February–June LSZ index is highly correlated with subsequent salinity variations in late summer [e.g., the reconstructed February–June LSZ data are correlated with the actual monthly LSZ indices of Jassby and others (1995) at 0.76 for July, 0.71 for August, 0.69 for September, and 0.67 for October, from 1956–2003]. The winter–spring period provides the principal natural climatic preconditioning for the summertime non-tidal salinity field, and is the season when large-scale ocean–atmospheric modes tend to induce interannual to decadal regimes on the precipitation and streamflow climatology of California.
7. The pure proxy precipitation-driven estimates of February–June low salinity position suggest that the natural hydroclimatic component of this estuarine habitat indicator has been approximately stationary over the past six centuries, subject to dramatic interannual and decadal scale maxima and minima, but not dramatically different from the unregulated hydroclimatic component of LSZ variability witnessed during the 20th century. These reconstructions do not cover the Medieval Era when various biological and geological proxies indicate that California may have experienced a fundamentally more negative water balance. These LSZ estimates are based entirely on the natural hydroclimatic forcing of tree growth, stream flow, and the resulting non-tidal position of the LSZ in the estuary, and they do not take into account the effects associated with ocean circulation, sea level rise, freshwater diversions, or anthropogenic climate changes on the natural runoff regime into the estuary.
8. Sea surface temperature and atmospheric circulation regimes over the North Pacific during the cool season are correlated with interannual variations in the reconstructed position of the LSZ. The most extreme wet years and LSZ minima have tended occur during very strong El Niño events, but droughts and salinity zone maxima do not

appear to occur during La Niña events.

9. Dense networks of long tree-ring chronologies have also been developed in the drainage basins of Delaware Bay, Chesapeake Bay, and Pamlico Sound (e.g., Cook and others 2007), and might be possible for Florida Bay. These tree-ring chronologies in the eastern United States do not tend to be as precipitation-sensitive as blue oak in California, but might nevertheless provide insight into physical and biological variability in those important Atlantic coast estuaries.

ACKNOWLEDGEMENTS

This research project was supported by the CALFED Ecosystem Restoration Program (grant number ERP02–P30). For property access and assistance, we thank the following institutions: California State Parks, National Park Service, Bureau of Land Management, USDA Forest Service, Turlock Irrigation District, Wind Wolves Preserve, Wildlands Conservancy, The Nature Conservancy, and the University of California Natural Reserve System. We also thank the following individuals: Ken Range, Carol Casey, Mary Moore, Peter Hujik, Kathryn Purcell, Walt Koenig, Mark Sturmburg, Dave Jigour, Dennis Sanfilippo, Pete Lucero, Tracy Brown, Jere Costello, Ken Murray, Henry Laussen, Lane and John Davis, Margorie Murphy, Jim Trumbly, Tom Leatherman, Steve Hill, Melody Fountain, Bob Stone, and Mr. Sinten. We thank Mark Borchert for extensive research advice, and Justin Pollan and Heather Fields for assistance. Noah Knowles, Jamie Anderson, and two anonymous reviewers supplied excellent advice and have helped to significantly improve the analyses and interpretations presented in this manuscript, for which we are very grateful.

REFERENCES

Allan RJ, Lindesay J, Parker D. 1996. El Niño–Southern Oscillation and climatic variability. Australia: CSIRO Publishing. 408 p.

Box GEP, Jenkins GW. 1976. Time series analysis: forecasting and control. San Francisco (CA): Holden–Day. 575 p.

[CDWR] California Department of Water Resources. 1999. DAYFLOW data. Sacramento (CA): Dept. of Water Resources. Available from: *http://iep.water.ca.gov/dayflow*.

Conomos TJ. 1979. San Francisco Bay: the urbanized estuary. In: Conomos TJ, Leviton AE, Berson M, editors. San Francisco (CA): AAAS, Pacific Division.

Cook ER. 1985. A time series analysis approach to tree-ring standardization [Ph.D. dissertation]. Available from: University of Arizona, Tucson. 171 p.

Cook ER, Peters K. 1981. The smoothing spline: a new approach standardizing forest interior tree-ring series for dendroclimatic studies. Tree Ring Bulletin 41:45–53.

Cook ER, Kairiukstis LA. 1990. Methods of dendrochronology: applications in the environmental Sciences. Dordrecht, Netherlands: Kluwer. 394 p.

Cook ER, Krusic P. 2008. ARSTAN program and user information. Available from: *http://www.ldeo.columbia.edu/res/fac/trl/public/publicSoftware.html*

Cook ER, Seager R, Cane MA, Stahle DW. 2007. North American drought: reconstructions, causes, and consequences. Earth Science Reviews 81:93–134.

Daly C, Halbleib M, Smith JI, Gibson WP, Doggett MK, Taylor GH, Curtis J, Pasteris PA. 2008. Physiographically-sensitive mapping of temperature and precipitation across the conterminous United States. International Journal of Climatology DOI: 10.1002/joc.1688.

Dettinger MD, Cayan DR, Diaz HF, Meko DM. 1998. North–south precipitation patterns in western North America on interannual-to-decadal timescales. Journal of Climate 11:3095–3111.

Dettinger MD, Cayan DR, 2003. Interseasonal covaribility of Sierra Nevada streamflow and San Francisco Bay salinity. Journal of Hydrology 277:164–181.

Douglass AE. 1941. Crossdating in dendrochronology. Journal of Forestry 39:825–828.

Draper NR, Smith H, 1981. Applied regression analysis, 2nd ed. New York (NY): John Wiley & Sons. 709 p.

Fritts HC. 1966: Growth-rings of trees: their correlation with climate. Science 154:973–979.

Fritts HC. 1976. Tree rings and climate. London: Academic Press. 567 p.

Granger OE. 1979. Increasing variability in California precipitation. Annals of the Association of American Geographers 69:533–543.

Grissino–Mayer HD. 2001. Assessing crossdating accuracy: a manual and tutorial for the computer program COFECHA. Tree-Ring Research 57:205–221.

Haston L, Michaelsen J. 1994. Long-term central coastal California precipitation variability and relationships to El Niño–Southern Oscillation. Journal of Climate 7:1373–1387.

Haston L, Michaelsen J. 1997. Spatial and temporal variability of Southern California precipitation over the last 400 years and relationships to atmospheric circulation patterns. Journal of Climate 10:1836–1852.

Hoerling MP, Kumar A. 2000. Understanding and predicting extratropical teleconnections related to ENSO. In: Diaz H, Markgraf V, editors. El Niño and the Southern Oscillation: multi-scale variability, and global and regional Impacts. Cambridge, UK: Cambridge University Press. p. 57–88.

Holmes RL. 1983. Computer-assisted quality control in tree-ring dating and measurement. Tree-Ring Bulletin 44:69–78.

[IMSL, Inc.] International Mathematical and Statistical Libraries, Inc. 1982. IMSL library reference manual, 9th ed. Vol. 2. Houston (TX): IMSL, Inc. p FTFREQ–1 to FTFREQ–5.

Ingram BL, Ingle JC, Conrad ME. 1996. A 2000 year record of Sacramento–San Joaquin river inflow to San Francisco Bay estuary, California. Geology 24:331–334.

Jassby AD, Kimmerer WJ, Monismith SG, Armor C, Cloern JE, Powell TM, Schubel JR, Vendlinski TJ. 1995. Isohaline position as a habitat indicator for estuarine populations. Ecological Applications 5:272–289.

Kaplan A, Cane MA, Kushnir Y, Clement AC, Blumenthal MB, Rajagopalan B. 1997. Analyses of global sea surface temperature 1856–1991. Journal of Geophysical Research 102:27835–27860. Update to 2005 available from: *http://www.cdc.noaa.gov/cdc/data.kaplan_sst*

Karl TR, Metcalf LK, Nicodemus ML, Quayle RG. 1983. Statewide average climatic history, California, 1897–1982. Historical Climatology Series 6–1, Asheville (NC): National Climatic Data Center. (As updated by NOAA).

Kimmerer W. 2004. Open water processes of the San Francisco Estuary: from physical forcing to biological responses. San Francisco Estuary and Watershed Science [Internet]. Available from: *http://www.escholarship.org/uc/item/9bp499mv*.

Kimmerer WJ, Murphy DD, Angermeier PL. 2005. A landscape-level model for ecosystem restoration in the San Francisco Estuary and its watershed. San Francisco Estuary and Watershed Science [Internet]. Available from: *http://www.escholarship.org/uc/item/5846s8qg*.

Knowles N. 2002. Natural and management influences on freshwater inflows and salinity in the San Francisco estuary at monthly to interannual scales. Water Resources Research 38:1289.

Kohler MA. 1949. On the use of double-mass analysis for testing the consistency of meteorological records for making required adjustments. Bulletin of the American Meteorological Society 30:188–189.

Malamud–Roam F, Dettinger MD, Ingram BL, Hughes MK, Florsheim JL. 2007. Holocene climates and connections between the San Francisco Bay estuary and its watershed: a review. San Francisco Estuary and Watershed Science [Internet]. Available from: *http://www.escholarship.org/uc/item/61j1j0tw*.

Meko DM, Stockton CW, Boggess WR. 1980. A tree-ring reconstruction of drought in southern California. Water Resources Bulletin 16:594–600.

Meko DM, Therrell MD, Baisan CH, Hughes MK. 2001. Sacramento River flow reconstructed to A.D. 869 from tree rings. Journal of the American Water Resources Association 37:1029–1039.

Meko DM, Stahle DW, Griffin RD, Knight TA. 2010. Inferring precipitation-anomaly gradients from tree rings. Quaternary International (in press).

Miller CB. 1983. The zooplankton of estuaries. In: Ketchum BH, editor. Estuaries and enclosed seas. Ecosystems of the World. Amsterdam: Elsevier. 500 p.

Monismith SG, Kimmerer W, Burau JR, Stacey MT. 2002. Structure and flow-induced variability of the subtidal salinity field in northern San Francisco Bay. Journal of Physical Oceanography 32:3003–3019.

Nichols FH, Cloern JE, Louma SN, Peterson DH. 1986. The modification of an estuary. Science 231:567–573.

Nobriga ML, Sommer TR, Fyrer F, Fleming K. 2008. Long-term trends in summertime habitat suitability for Delta smelt (*Hypomesus transpacificus*). San Francisco Estuary and Watershed Science [Internet]. Available from: *http://www.escholarship.org/uc/item/5xd3q8tx*

Peterson DH, Cayan DR, Festa JF, Nichols FH, Walters RA, Slack JV, Hager SE, Schemel LE. 1989. In: Peterson DH, editor. Aspects of climate variability in the Pacific and the western Americas. Geophysical Monograph Series 55. Washington, D.C.: American Geophysical Union.

Peterson DH, Cayan DR, DiLeo J, Noble MA, Dettinger MD. 1995. The role of climate in estuarine variability. American Scientist 83:58–67.

Reisner M. 1988. Cadillac desert. New York: Penguin Books.

Uncles RJ, Peterson DH. 1995. A computer model of long-term salinity in San Francisco Bay: sensitivity to mixing and inflows. Environment International 21:647–656.

SAS® Institute Inc. 1985. SAS® user's guide: Basics, Version 5. Cary, NC: SAS Institute Inc. 1290 p.

SAS® Institute Inc. 1999: SAS/STAT® user's guide, Version 8. Ch. 30, The GLM Procedure. Cary, NC: SAS® Institute Inc., 1467–1636.

Schemel LE, Harmon DD, Hager SW, Peterson DH. 1984. Response of northern San Francisco Bay to riverine inputs of dissolved inorganic carbon, silicon, nitrogen, and phosphorus. In: Kennedy VS, editor. The estuary as a filter. New York: Academic Press. 511 p.

Smith CA, Sardeshmukh P. 2000. The effect of ENSO on the intraseasonal variance of surface temperature in winter. International Journal of Climatology 20:1543–1557.

Stahle DW, Therrell MD, Cleaveland MK, Cayan DR, Dettinger MD, Knowles N. 2001. Ancient blue oak reveal human impact on San Francisco Bay salinity. Eos, Transactions of the American Geophysical Union 82(12)141:144–145.

Starratt SW. 2007. Diatoms in estuaries and tidal marshes. The Paleontological Society Papers 13:85-110.

[SWRCB] State Water Resources Control Board. 1995. Water quality control plan for the San Francisco Bay.Sacramento–San Joaquin Delta estuary. 95–1 WR. California Environmental Protection Agency. 55 p. Available from: *http://www.waterrights.ca.gov/baydelta/d1614.htm*

Steel RGD, Torrie JH. 1980. Principles and Procedures of Statistics, 2nd ed., New York: McGraw–Hill. 633 p.

Stokes MA Smiley TL. 1996. An introduction to tree-ring dating. 2nd ed. Tuscon (AZ): University of Arizona Press. 73 p.

Torrence C, Compo GP. 1998. A practical guide to wavelet analysis. Bulletin of the American Meteorological Society 79:61–78.

Viessman W, Harbaugh TE, Knapp JW. 1972. Introduction to hydrology. New York (NY): Intext Educational Publishers. 415 p.

Zhang Y, Wallace JM, Battisti DS. 1997. ENSO-like interdecadal variability: 1900–93. Journal of Climate 10:1004–1020.